International Journal of Current Engineering and Technology
E-ISSN 2277 – 4106, P-ISSN 2347 – 5161

Available at http://inpressco.com/category/ijcet

Research Article

Modification of calcination temperature of NiO/C nanocomposite electrode materials for supercapacitor application

[1]Seemab Hussnain, [1]Muhammad Zeeshan, [1]Shahid Iqbal, [2]Muhammad Umer, [3]Muhammad Hamad Safder, [3]Asad Fiaz and [*]Muhammad Qadeer Alam

[1]Department of Physics, University of Agriculture Faisalabad, Pakistan
[2]Department of Chemistry, Minhaj University Lahore, Pakistan
[*3]Department of Physics, Government College University Layyah, Pakistan

Received 01 Sept 2022, Accepted 20 Sept 2022, Available online 26 Sept 2022, **Vol.13, No.5 (Sept/Oct 2022)**

Abstract

Synthesizing metal oxide nanomaterials for energy storage applications and optimizing their electrochemical performance is critical for developing next generation energy solutions. In this study, nickel hydroxide nanomaterials were synthesized via precipitation and microwave methods and utilized as pseudo-capacitor electrodes. The precipitation method employing starch as a capping agent yielded nickel hydroxide exhibiting a maximum specific capacitance of 333 Fg^{-1}. The nickel hydroxide can be converted to nickel oxide/carbon (NiO/C) by calcination at higher temperatures. Electrochemical supercapacitor performance of NiO/C synthesized at different calcination temperatures (400, 500, 600 °C) was optimized. NiO/C calcined at 500 °C exhibits a maximum specific capacitance value of 450 Fg^{-1} at a scan rate of 5 $mV.s^{-1}$. To determine the structural properties XRD technique was used. The identification of functional groups in synthesized nanomaterials was investigated by the FTIR technique. FESEM was employed to examine the morphological analysis of synthesized nanomaterials. Elemental composition in synthesized materials was examined by using the EDS. The electrochemical potential was studied by using CV, GCD, and EIS techniques.

Keywords: *Metal oxide nanomaterials, Microwave methods, Electrochemical supercapacitor performance*

1. Introduction

Energy storage technologies play a vital role in enabling sustainable energy solutions and powering modern societies. Among various options, electrochemical supercapacitors have attracted significant interest due to their high-power density, long lifespan, and ability to bridge the gap between batteries and conventional capacitors. Electrochemical capacitors, also known as supercapacitors, have attracted significant attention in recent years due to their ability to bridge the gap between conventional capacitors and batteries [1]. They exhibit higher power densities than batteries and higher energy densities than conventional dielectric capacitors [2]. Based on the energy storage mechanism, supercapacitors are classified as electric double-layer capacitors (EDLCs) and pseudocapacitors [3]. Supercapacitors store charge either via non-Faradaic ion adsorption/ desorption at electrode/electrolyte interfaces (electric double-layer capacitors, EDLCs) or through Faradaic surface redox reactions (pseudocapacitors). EDLCs rely on ion adsorption/desorption at the interface between electrode and electrolyte [4].

Carbon materials with high surface area such as activated carbon are commonly used as EDLC electrodes [5]. Pseudocapacitors utilize fast and reversible Faradaic redox reactions on the surface of certain transition metal oxides and conducting polymers to provide higher capacitance [6]. Transition metal oxides such as ruthenium oxide (RuO_2), manganese oxide (MnO_2), nickel oxide (NiO), and cobalt oxide (Co_3O_4) exhibit excellent pseudocapacitive behavior [7,8]. Pseudocapacitive transition metal oxides, such as ruthenium oxide, have been widely investigated as electrode materials due to their higher energy densities compared to carbon-based EDLCs [12,19]. However, the high cost and scarce availability of ruthenium hamper its widespread application. Recent research has focused on developing inexpensive pseudocapacitive metal oxides based on abundant elements such as nickel. Nickel oxide (NiO) is a promising candidate, possessing desirable properties including high theoretical specific capacitance, good chemical and thermal stability, and low toxicity [9]. Various synthesis methods have been applied to fabricate nanostructured NiO for enhanced electrochemical performance. However, further improvements are still needed to optimize its

*Corresponding author's ORCID ID: 0009-0000-2799-682X
DOI: https://doi.org/10.14741/ijcet/v.13.5.2

capacitance. Various methods have been applied to produce nanoscale transition metal oxides for supercapacitor applications [14]. Precipitation is a simple method for preparing nickel hydroxide nanoparticles. Starch is commonly used as a capping agent to control particle size and morphology [15]. calcination of nickel hydroxide yields NiO while preserving the nanostructure [16]. Doping with electroactive elements is a viable strategy, as it can modulate the material's electronic structure and induce pseudocapacitive charge storage mechanisms. Device design is another key factor affecting energy storage performance. Symmetric supercapacitors using a single electrode material have simpler fabrication but energy is limited by voltage window [24]. Asymmetric designs pair a battery-type material with a capacitor-type one to utilize their respective potentials [25]. Activated carbon is commonly used alongside transition metal oxides in asymmetric devices [26]. Xia et al. [3] reported the porous NiO to maintain its morphology even after 4000 continuous cycles and to remain unaffected by the damage caused by volume expansion during continuous cycling process. Even though thin film morphology shows higher capacitance, powders are desirable due to low volumetric density of thin films. Carbon coating on nickel oxide enhances the supercapacitor performance of the electrode material. Fan et al. [4] recently reported increased supercapacitor behavior of carbon-encapsulated nickel oxide. They reported the maximum specific capacitance of 988.7 $Fg^{-1}$for carbon encapsulated nickel oxide whereas, hollow NiO spheres exhibit 594.4 Fg^{-1}. They attributed the improved performance to the encapsulation. Huang et al. [5] also reported that net-structured NiO-C nanocomposites exhibit excellent electrochemical properties. In this work, we report the development of nanostructured nickel oxide/carbon powders synthesized via precipitation and microwave-assisted methods. Their use as symmetric and asymmetric supercapacitor electrodes is evaluated to maximize energy storage capabilities. This work provides insights towards optimizing inexpensive transition metal oxide materials for electrochemical energy applications.

2. Experimental

2.1 chemicals

Analytical grade nickel nitrate hexahydrate ($Ni(NO_3)_2 \cdot 6\ H_2O$) and Ammonium hydroxide (NH_4OH) were purchased from Sigma-Aldrich, 99.8%. Dextrose and starch were purchased from Merck, 98%. All chemicals are used as received without further purification.

2.2 Preparation of NiO/C materials

Nickel hydroxide nanoparticles were synthesized via precipitation by dissolving starch, nickel nitrate, and dextrose in water, then adding ammonia to raise the 10 pH. The precipitate was washed, dried at 60°C, and ground. Heat treatment yielded nickel oxide/carbon (NiO/C) nanocomposites by calcining at 400-600°C, denoted as NiO/C-4, NiO/C-5, NiO/C-6 based on temperature. Characterization revealed morphological and structural changes after calcination at different temperatures.

2.3 Characterization tools

The synthesized materials were characterized using various techniques. XRD was conducted using a PRO X-ray diffractometer with a CuKα X-ray source to analyze crystallinity from 10-80° 2θ. FTIR spectroscopy was recorded by using a Perkin Elmer spectrometer to identify functional groups from 400-4000 cm^{-1}. TGA (EXSTAR-6200) was performed from room temperature to 800°C under air to study thermal stability. FESEM (Joel jsm-6701f) and TEM (H-7100 KVA) imaging revealed morphological changes after calcination at different temperatures. EDS (Quantax-200) confirmed the elemental composition.

2.4 Electrochemical studies

Electrochemical characterization of the synthesized samples was conducted using a three-electrode cell with CHI-660D instruments. NiO/C served as the working electrode, Pt as the counter electrode, and Ag/AgCl as the reference electrode, with 2.0 M KOH electrolyte. Cyclic voltammetry, galvanostatic charge-discharge, and electrochemical impedance spectroscopy techniques were employed to evaluate the supercapacitor properties.

2.5 Electrode preparation

Graphite sheets were used as current collectors. They were degreased with acetone/water and etched in 0.1 M HCl. Working electrodes were prepared by mixing 80 wt% NiO/C nanomaterials, 15 wt% active carbon, and 5 wt% PTFE binder in ethanol. The slurry was coated on 1 cm^2 graphite sheets and dried at 80°C for 6 hours, with an active material loading of 0.8 mg.

3. Results and discussions

3.1 Thermogravimetry and structural analysis

Thermal gravimetric and structural analysis provides information on phase shifts, possible sample decomposition, and the purity of NiO/C composite materials. Thermal and structural analysis was conducted on NiO/C nanocomposites Fig. 1. TGA from RT to 800°C under air Fig. 1a revealed a three-step weight loss (200 °C, 200 °C-360 °C and 360 °C-800 °C) attributed to dehydration and decomposition. FTIR Fig. 1b confirmed the conversion of $Ni(OH)_2$ to NiO between 200-360°C. The band positions at 3423 cm^{-1}[6], 1625 cm^{-1}[7], 1357 cm^{-1}[7], 1016 cm^{-1},617 cm^{-1} [7], and 446 cm^{-1} [6] are assigned to the interlayer O-H stretching vibration, vibrations of H_2O molecules,

interlayer NO_3^- molecule, C-O bond vibration, vibrations of δNi–OH, and Ni-O, respectively. The FTIR spectra of materials heated beyond 400 °C exhibited bands confined to Ni-O. The temperature rises as the carbon begins to burn off. XRD Fig. 1c showed crystalline NiO and carbon phases (NiO/C-4, NiO/C-5, and NiO/C-6) in samples calcined at 400-600°C. Carbon content decreased while NiO crystallinity (18-22 nm) and grain size increased over this range, indicating phase evolution.

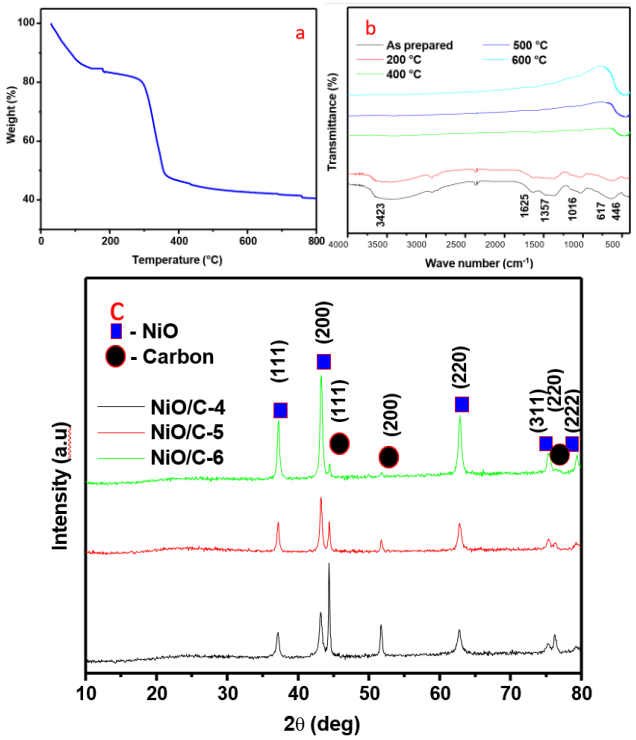

Fig. 1 a) TGA of uncalcined sample, b) FTIR spectrum of samples calcined at different temperatures and c) XRD pattern of NiO/C samples.

3.2 Morphological and elemental composition analysis

Morphological analysis techniques like scanning electron microscopy or optical microscopy allow close examination of a material's microscopic structure, texture, and physical characteristics. It reveals details about size, shape, structure, and how components are arranged and structured together. Elemental composition analysis identifies and quantifies the constituent elements that comprise a material. Techniques such as X-ray fluorescence spectroscopy, energy-dispersive X-ray spectroscopy, or inductively coupled plasma-mass spectrometry are used to determine the relative percentage of each element present. These analytical methods provide important information about a material's microstructure and chemical properties at the microscopic level. Morphological analysis sheds light on physical characteristics while elemental composition identifies molecular components. Together they allow for more comprehensive characterization of complex materials.

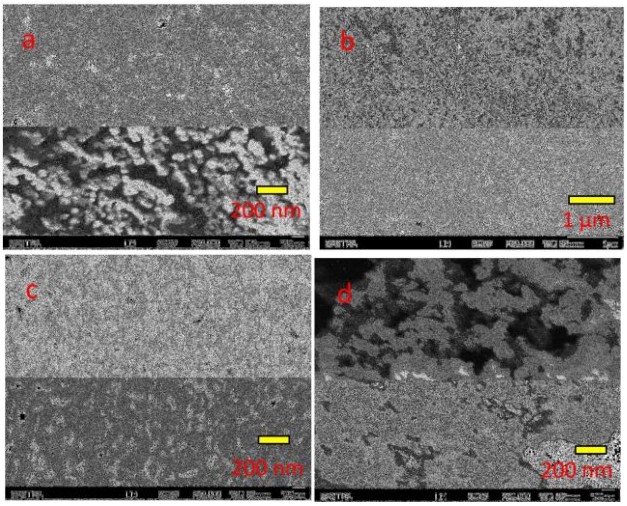

Fig. 2 FESEM images of samples calcined at (a) 400 °C, (b, c) 500 °C, and (d) 600 °C.

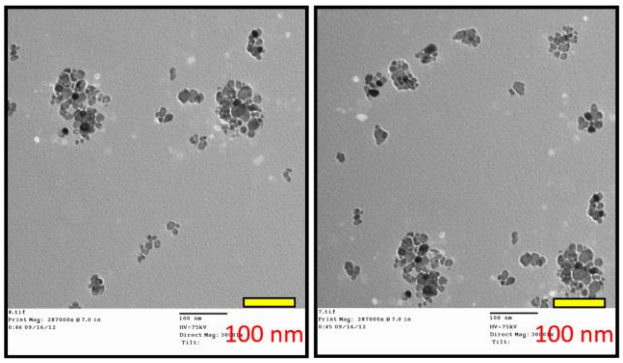

Fig. 3 TEM images of NiO/C-5 sample.

To evaluate the morphological features of the samples, FESEM images of the samples have been obtained and studied. Fig. 2 shows the FESEM images of NiO/C-4, NiO/C-5, and NiO/C-6 samples. From the FESEM images, it is observed that the morphology depends on the calcination temperature. The image corresponding to the samples calcined at 400 °C reveals the formation of spherical particles with some uneven pores. These uneven pores are probably due to smaller quantities of carbon burn-off. Samples calcined at 500 °C. Fig.2b shows a mesh-like porous morphology of NiO/C due to the removal of carbon at a uniform rate. At an increased resolution Fig. 2c a mesh-like network formation along with pores could be identified. Fig. 3 shows TEM images of the NiO/C-5 sample. TEM images show the porous nature of the NiO/C samples. FESEM image of sample calcined at 600 °C. Fig. 2d exhibits reduced porosity and even some degree of agglomeration of the network to form large clusters. Generally, increasing the calcination temperature damages the specific morphology [11]. The porous nature appears to be damaged at elevated calcination temperatures.

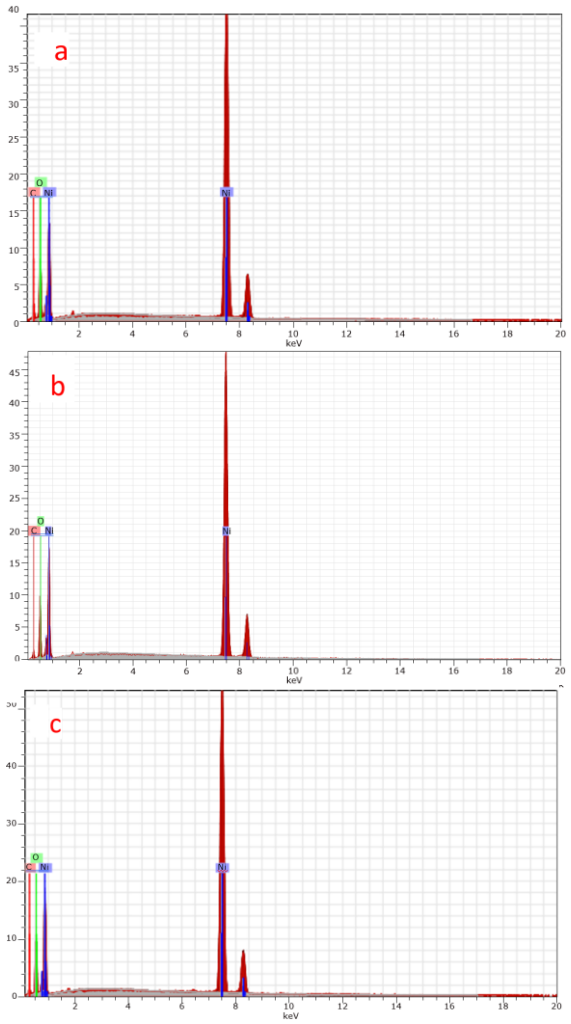

Fig. 4 EDS spectra of sample calcined at (a) 400 °C, (b) 500 °C and (c) 600 °C.

Fig. 4 shows the EDS spectrum of the NiO/C nanocomposites. NiO/C-4, NiO/C-5 and NiO/C-6 samples reveal the presence of 13%, 9%, and 6% of carbon by weight, respectively. The Ni/O atom ratio from EDS analysis is close to unity confirming the formation of NiO without any stoichiometric variations.

3.3 Electrochemical studies

Electrochemical properties are dependent on material structure and morphology. Calcination temperature is important for controlling structure and morphology. Optimizing calcination temperature is essential for superior electrochemical performance. Electrochemical measurements including cyclic voltammetry, charge-discharge, and electrochemical impedance analysis were conducted to characterize the supercapacitor performance of nanocomposite electrodes (NiO/C-4, NiO/C-5, NiO/C-6).

Cyclic voltammetry within 0-0.5 V vs Ag/AgCl in 2.0 M KOH electrolyte was performed. Fig. 5(a-c) shows the CV curves of NiO-4, NiO-5, and NiO-6 electrodes at different scan rates. Well-defined redox peaks indicate a Faradaic process in addition to electric double-layer capacitance. The asymmetric anodic and cathodic peaks suggest the kinetic irreversibility of the redox process. Charge storage in NiO electrodes involves surface redox reactions.

$$NiO + zOH^- \Longleftrightarrow zNiOOH + (1-z)\,NiO + ze^- \quad (1)$$

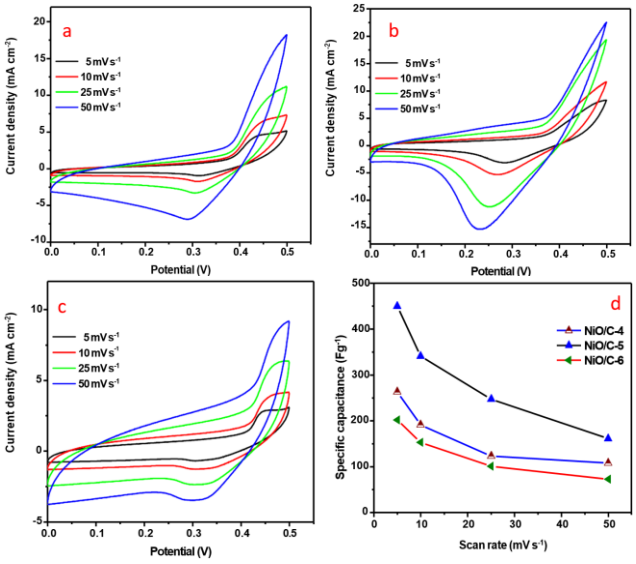

Fig. 5 CV traces of (a) NiO/C-4, (b) NiO/C-5, and (c) NiO/C-6 electrodes at different scan rates. (d) Variation of specific capacitance with scan rate

The specific capacitance (Cs) values of NiO/C are obtained using the following equation [16]. The area under the curve of NiO/C-5 is higher compared to that of NiO/C-4 and NiO/C-6. This difference can be attributed to the mesh-like porous structure observed in NiO/C-5 through FESEM analysis, which facilitates fast intercalation and deintercalation of the active species. Although NiO/C-4 also possesses a porous structure, NiO/C-5 exhibits a larger area due to its highly porous nature. On the other hand, NiO/C-6 demonstrates a smaller area due to poor morphological features and aggregation of the porous structure.

$$C_s = \frac{Q}{m\Delta v} \quad (2)$$

The specific capacitance (Cs) values were calculated using the formula [16]. For NiO/C-4, NiO/C-5, and NiO/C-6, the estimated specific capacitance values (at a scan rate of 5 $mV.s^{-1}$) are 263, 450, and 202 Fg^{-1}, respectively. The dependence of specific capacitance on scan rate is illustrated in Fig. 5d. It is observed that specific capacitance values decrease as the scan rate increases. This is because, at high scan rates, the OH^- ions primarily access the outer surface of the electrode, whereas, at low scan rates, the OH^- ions can intercalate both the outer and inner pore surfaces effectively. As the scan rate increases, the available time for ion

diffusion decreases, resulting in reduced charge storage. This limited accessibility of OH^- ions leads to a decrease in specific capacitance values at higher scan rates [17]. The carbon coating in the NiO/C nanocomposites plays a significant role in enhancing specific capacitance. It provides double-layer capacitance and facilitates conducting pathways for ion transfer, thereby increasing specific capacitance. Additionally, the carbon coating helps suppress the aggregation of nickel oxide [4, 18].

To assess the cyclic behavior and stability of the NiO/C samples calcined at various temperatures, charge-discharge measurements were conducted at different current densities within a voltage window of -0.05 to 0.45 V, using 2.0 M KOH as the electrolyte. Fig. 6(a-c) illustrates the charge-discharge curves of NiO/C-4, NiO/C-5, and NiO/C-6. The specific capacitance (Cs) values were determined using the formula [16].

$$C_s = \frac{i\Delta t}{m\Delta v} \quad (3)$$

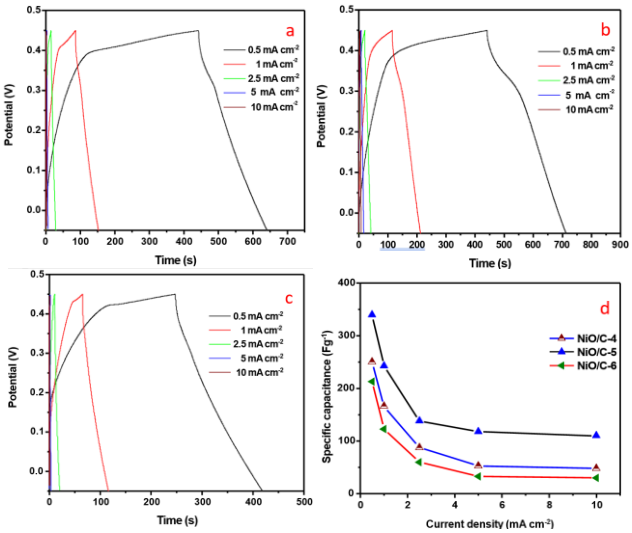

Fig. 6 Charge-discharge curves of (a) NiO/C-4, (b) NiO/C-5, and (c) NiO/C-6 electrodes at different current densities. (d) Variation of specific capacitance with current density.

The observed trend in specific capacitance measurements is consistent with the findings from cyclic voltammetry (CV) experiments. The porous structure of NiO/C-5 serves as a buffering reservoir for OH^- ions, reducing the diffusion lengths for electrolyte ions and ensuring sufficient contact between electrolyte ions and the larger surface area of the electroactive NiO/C electrode [19]. The charging and discharging curves at different current densities exhibit asymmetry due to the kinetic irreversibility of OH^- ions on the electrode surface [9]. Fig. 6d depicts the variation in specific capacitance with different current densities for NiO/C-4, NiO/C-5, and NiO/C-6 electrodes.

The capacitance of the NiO/C electrodes decreases with increasing current densities. This can be attributed to the voltage (IR) drop caused by the equivalent series resistance of the capacitor, which increases with higher current densities and consequently reduces the specific capacitance of the electrode. At low current densities, ions have sufficient time to intercalate and deintercalate, allowing access to both the outer surface and inner pores of the electrode. However, at high current densities, ions primarily access the outer surface, resulting in a decrease in specific capacitance.

For practical applications of supercapacitors, cyclic stability at higher current densities is crucial. Therefore, the NiO/C-5 electrodes were subjected to 500 continuous charge-discharge cycles at a current density of 10 $mA.cm^{-2}$. Fig. 7 presents the profile of specific capacitance values over the course of cycling. The stability curve demonstrates that the NiO/C-5 electrode exhibits excellent cycling stability, retaining 91% of the initial capacitance even after 500 charge-discharge cycles. In a study by Fan et al. [4], a specific capacitance retention of 90.7% was reported after 1000 charge-discharge cycles. Hence, the NiO/C-5 electrode proves to be a suitable material for supercapacitor applications.

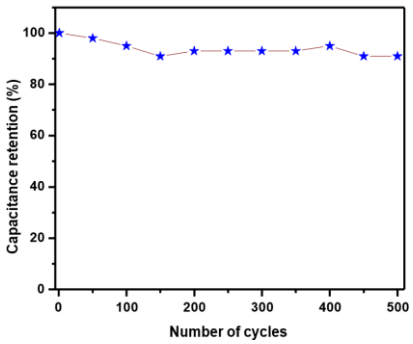

Fig. 7 Cyclic stability charge-discharge curve of NiO/C-5 electrode at 10 $mA.cm^{-2}$

In terms of electrochemical performance, it is desirable to design supercapacitors with low equivalent series resistance, as they are intended for power applications. The impedance plots of the NiO/C-4, NiO/C-5, and NiO/C-6 electrodes were obtained in a frequency range of 0.01 to 100 kHz at a bias potential of 0.4 V. These plots are shown in Fig. 8(a-c). The inset of Fig. 8b illustrates the equivalent fitting circuit used for the NiO/C electrodes, where Rs represents the solution resistance, Rct is the charge-transfer resistance, Cdl denotes the double-layer capacitance, and W corresponds to the Warburg impedance, as discussed previously. At higher frequencies, the intersection on the real axis represents the solution resistance, which was determined to be 1.41 Ω, 2.66 Ω, and 1.39 Ω for NiO/C-4, NiO/C-5, and NiO/C-6 electrodes, respectively. This solution resistance is a combination of various factors, including ionic and electronic resistances, intrinsic resistance of the NiO/C electrode, and diffusive as well as contact resistance at the interface between the NiO/C electrode and the current collector [20].

The semicircular feature observed in the high-frequency region corresponds to the charge-transfer resistance, Rct. This resistance is associated with the electroactive surface area of the electrode, resulting from the Faradic redox process of the NiO/C electrodes involving the exchange of OH^- ions [20]. The values of the charge-transfer resistance were determined to be 1.09 Ω, 0.59 Ω, and 1.18 Ω for NiO/C-4, NiO/C-5, and NiO/C-6 electrodes, respectively. The lower Rct value for NiO/C-5 can be attributed to the enhanced diffusivity of OH^- ions within the porous electrode structure [2]. This observation is supported by the mesh-like structure observed in the scanning electron microscopy (SEM) images.

The linear portion observed in the low-frequency region corresponds to the Warburg resistance, which represents the diffusive resistance of OH^- ions within the NiO/C electrodes. The specific capacitance values of the NiO/C electrodes were calculated from the impedance data using the equations provided in references [21, 22].

$$C_s = \frac{1}{2\pi f Z''} \quad (4)$$

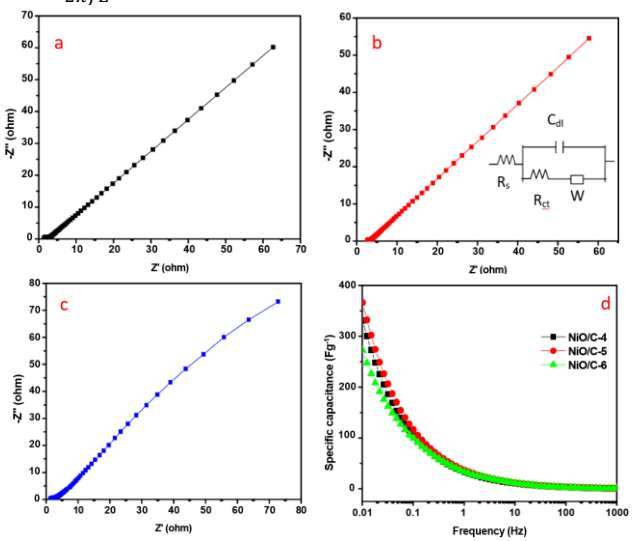

Fig. 8 Impedance plot of (a) NiO/C-4, (b) NiO/C-5 and (c) NiO/C-6 electrodes at 0.4 V. Inset of fig. b shows the equivalent fitting circuit. (d) Frequency-dependent specific capacitance of NiO/C electrodes.

Fig. 8d shows the frequency-dependent specific capacitance curve of NiO/C electrodes. The specific capacitance values for NiO/C-4, NiO/C-5, and NiO/C-6 electrodes are 331, 366, and 272 Fg^{-1}, respectively. These results are in good agreement with the cyclic voltammetric and charge-discharge results.

Conclusion

NiO/C nanocomposites were prepared at different calcination temperatures. NiO/C-5 shows a uniform porous structure. The NiO/C-5 electrode exhibits a maximum specific capacitance of 450 Fg^{-1} at 5 $mV.s^{-1}$. The NiO/C-5 electrode has advantages over NiO/C-4 and NiO/C-6, as the uniform porous structure facilitates a greater number of active sites for ion access. The charge transfer resistance is low for NiO/C-5. It further 91% of the capacity after 500 cycles. This NiO/C-5 electrode exhibits high specific capacitance and low charge transfer resistance. Hence, NiO/C electrodes calcined at 500 °C are the best suited for supercapacitor applications.

Reference

[1] Li, Y., Zhao, X., Zhang, Q., & Chen, D. (2011). Porous NiO/C composite electrodes for supercapacitor applications. Langmuir, 27(21), 6458.
[2] Zhang, J., Kong, L. B., Cai, J. J., Li, H., Luo, Y. C., & Kang, L. (2010). Hierarchical porous NiO nano/microspheres: Synthesis, characterization and application in supercapacitors. Microporous and Mesoporous Materials, 132, 154.
[3] Xia, X. H., Tu, J. P., Wang, X. L., Gu, C. D., & Zhao, X. B. (2011). Hierarchical porous NiO/Ni nanostructures: Synthesis, characterization and application in supercapacitors. Journal of Materials Chemistry, 21(2), 671.
[4] Fan, L., Tang, L., Gong, H., Yao, Z., & Guo, R. (2012). Hierarchical porous NiO microspheres assembled by nanosheets for high-performance supercapacitors. Journal of Materials Chemistry, 22(33), 16376.
[5] Huang, X. H., Tu, J. P., Zhang, C. Q., & Xiang, J. Y. (2007). Supercapacitive behavior of nanostructured NiO thin film electrodes. Electrochemistry Communications, 9(5), 1180.
[6] Liu, X. M., Zhang, X. G., & Fu, S. Y. (2006). Preparation and electrochemical capacitance of porous NiO film. Materials Research Bulletin, 41(4), 620.
[7] Fu, G. R., Hu, Z. A., Xie, L. J., Jin, X. Q., Xie, Y. L., Wang, Y. X., Zhang, Z. Y., Yang, Y. Y., & Wu, H. Y. (2009). Preparation and characterization of porous NiO film and its electrochemical capacitance. International Journal of Electrochemical Science, 4, 1052.
[8] Srinivasan, V., & Weidner, J. W. (2000). Electrochemical capacitance of porous nickel oxide electrodes. Journal of the Electrochemical Society, 147(3), 880.
[9] Meher, S. K., & Rao, G. R. (2011). Hierarchical porous NiO nanostructures: Synthesis, characterization, and supercapacitor performance. ACS Applied Materials & Interfaces, 3(6), 2063.
[10] Liu, P., Cao, Y. L., Wang, C. X., Chen, X. Y., & Yang, G. W. (2008). Hierarchical porous NiO nanostructures for high-performance supercapacitors. Nano Letters, 8(8), 2570.
[11] Lee, J. W., Ahn, T., Kim, J. H., Ko, J. M., & Kim, J. D. (2011). Porous nickel oxide film with micro/mesopores for supercapacitors. Electrochimica Acta, 56(12), 4849.
[12] Zhang, X., Shi, W., Zhu, J., Zhao, W., Ma, J., Mhaisalkar, S., Maria, T. L., Yang, Y., Zhang, H., Hng, H. H., & Yan, Q. (2010). Hierarchical porous nickel oxide/carbon microtube nanocomposites for high-performance supercapacitors. Nano Research, 3(9), 643.
[13] Sun, X., Wang, G., Hwang, J. Y., & Lian, J. (2011). Mesoporous NiO nanosheets with enhanced capacitive properties for supercapacitors. Journal of Materials Chemistry, 21(43), 16581.
[14] Xiong, S., Yuan, C., Zhang, X., & Qian, Y. (2011). Hierarchically porous NiO nanosheets for supercapacitors. CrystEngComm, 13(2), 626.
[15] Meher, S. K., Justin, P., & Rao, G. R. (2011). Hierarchical porous NiO nanostructures: Synthesis, characterization, and supercapacitor performance. Nanoscale, 3(2), 683.
[16] Yan, J., Khoo, E., Sumboja, A., & Lee, P. S. (2010). Achieving high capacitance in nickel oxide supercapacitor

electrodes byintegrating hierarchical nanostructures. ACS Nano, 4(7), 4247.
[17] Patil, U. M., Gurav, K. V., Fulari, V. J., Lokhande, C. D., & Oh, S. J. (2009). Facile synthesis and electrochemical characterization of nanostructured NiO thin films for supercapacitor applications. Journal of Power Sources, 188(2), 338.
[18] Nagamuthu, S., Vijayakumar, S., & Muralidharan, G. (2013). NiO nanoparticles as an efficient electrode material for supercapacitors. Energy & Fuels, 27(6), 3508.
[19] Wang, D. W., Li, F., Liu, M., Lu, G. Q., & Cheng, H. M. (2008). 3D aperiodic hierarchical porous graphitic carbon material for high-rate electrochemical capacitive energy storage. Angewandte Chemie International Edition, 47(20), 373.
[20] Wu, M. S., & Hsieh, H. H. (2008). Preparation and electrochemical properties of mesoporous NiO films as electrode materials for supercapacitors. Electrochimica Acta, 53(8), 3427.
[21] Conway, B. E. (1999). Electrochemical Supercapacitors: Scientific Fundamentals and Technological Applications. Kluwer Academic/Plenum Publishers.
[22] Wang, G., Zhang, L., & Zhang, J. (2012). A review of electrode materials for electrochemical supercapacitors. Chemical Society Reviews, 41(2), 797.
[23] Ren, Y., Ma, Z., Bruce, P. G., & Liu, Z. (2013). Nanosized tunneled structure assembled from nickel hydroxide nanosheets for high-rate pseudocapacitive electrodes. Nano letters, 13(11), 5588-5593.
[24] Beidaghi, M., & Gogotsi, Y. (2014). Capacitive energy storage in micro-scale devices: recent advances in design and fabrication of micro-supercapacitors. Energy & Environmental Science, 7(3), 867-884.
[25] Yang, P., Tarascon, J. M., & Guerfi, A. (2013). Review—The design, synthesis, and recycling of lithium-ion battery electrodes and electrolytes. Journal of The Electrochemical Society, 160(10), A2179-A2188.
[26] Zhang, Y. H., Ang, K. P., & Yang, A. X. (2009). Flexible asymmetric supercapacitors based on activated carbon and cobalt oxide hydroxide films on stainless steel. Nanotechnology, 20(50), 505402.